Available online at www.sciencedirect.com

ScienceDirect

IFAC PapersOnline CONFERENCE PAPER ARCHIVE

IFAC PapersOnLine 53-2 (2020) 11422–11427

Robust Control of Fluidized Bed Layering Granulation

Christoph Neugebauer * **Carsten Seidel** * **Stefan Palis** *,** **Achim Kienle** *,***

* *Institute for Automation, Otto von Guericke University, Magdeburg, Germany (e-mail: stefan.palis@ovgu.de)*
** *Moscow Power Engineering Institute, Moscow, Russia*
*** *Max Planck Institute for Dynamics of Complex Technical Systems, Magdeburg, Germany*

Abstract: This contribution is concerned with control of fluidized bed layering granulation with external sieve-mill-cycle. It is well-known that this configuration is sensitive with respect to variations in the operating conditions and supplied material properties. Therefore, control is needed to achieve desired particle properties over a wide range of process conditions. In this contribution H_∞-control is applied in order to control the process. In contrast to preceding works, the coupling between the particle and the fluid phase is taken into account. Furthermore, in addition to the Sauter diameter of the particle size distribution, the apparent particle porosity is controlled, which is of great importance for practical applications.

Keywords: Particulate processes, robust control

1. INTRODUCTION

Fluidized bed layering granulation is an important particulate process, whose purpose is to transform a liquid raw material into a solid product. It is operated in a fluidized state, i.e. the particle bed is fluidized by supplying an air stream. Injecting a solution or suspension to the fluidized particle bed results in a wetting of the particle surface. This liquid layer is then dried and forms therefore a new solid layer resulting in a particle growth. In order to achieve a constant particle production the granulation process can be combined with a sieving box, separating the desired product size from to small or to big particles, and a mill, generating new nuclei from oversized particles.

As has been investigated for example by Dreyschultze et al. (2015), Schmidt et al. (2017), Neugebauer et al. (2017) and Neugebauer et al. (2019) the described configuration may lead to instabilities, resulting in the occurrence on nonlinear oscillations of the particle size distribution. These are in general undesired. To overcome this problem different feedback control approaches have been proposed. In Cotabarren et al. (2015) decentralized PI-controllers are designed for a multi-chamber granulation process. Robust H_∞-loop shaping controllers have been investigated in Palis and Kienle (2012, 2013) for two continuous granulation processes with internal and external product classification. For the later a nonlinear discrepancy-based controller has been proposed in Palis and Kienle (2014). In order to cope with uncertainties and reduce controller complexity a simple adaptive model-free control scheme has been proposed in Palis (2018) for a continuous granulation process with internal classification. It should be mentioned, that the focus in previous contributions has been on the particle phase not taking into account the heat and mass transfer with the gas and liquid phase. Although, this is a reasonable first step, newer experimental investigations (e.g. Rieck et al. (2015) and Diez et al. (2018)) show that the coupling between these phases may have a great influence on product properties. For instance, shell porosity ϵ_{shell} and apparent particle porosity ϵ_{p}, two important particle properties, depend on the thermal process conditions. A first model accounting for the bidirectional coupling between the particles and the fluid phase has been proposed in Neugebauer et al. (2018).

Therefore, in this contribution, a robust control approach is applied to control a fluidized bed layering granulation taking into account the heat and mass transfer, i.e. the interchange between the gas phase of the fluidization air, the liquid phase of the solution or suspension and the solid phase of the particle bed.

2. DYNAMIC PROCESS MODEL

Depending on the focus, particulate processes can be described by different model paradigms. In this contribution, the focus is on the time-evolution of the whole population of particles, in contrast to the behavior of a single particle. This can be described by a population balance model, where the internal coordinate is the characteristic particle size L. In fluidized bed layering granulation, the change in the particle size distribution $n\,(t, L)$ is mainly due to particle growth and the feed $\dot{n}_{\text{in}}$ and withdrawal $\dot{n}_{\text{out}}$ of particles. Additional effects like nucleation due to spray drying, agglomeration or particle breakage can in general been neglected.

$$\frac{\partial n\,(t, L)}{\partial t} = -G\frac{\partial n}{\partial L} + \dot{n}_{\text{in}} - \dot{n}_{\text{out}} \tag{1}$$

10.1016/j.ifacol.2020.12.578

In the given configuration, particles are continuously withdrawn from the granulation chamber and fed to a sieving box to remove product and oversized particles. The oversized particles are then ground and fed back into the granulation chamber. The overall process scheme is depicted in Fig. 1.

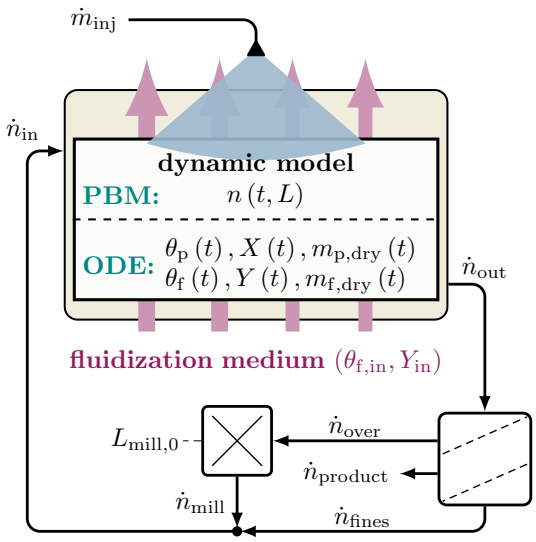

Fig. 1. Flow sheet of the investigated fluidized bed layering granulation with screen-mill-cycle.

Assuming spherical particles and an equal distribution of the injected liquid on the particle surface the growth rate G (Mörl et al. (2007)) is given as follows

$$G\left(n, \dot{m}_{\text{inj}}, \epsilon_{\text{shell}}\right) = \frac{2 x_{\text{inj}} \dot{m}_{\text{inj}}}{\left(1-\epsilon_{\text{shell}}\right) \rho_{\text{s}} \pi \mu_2(n)}. \tag{2}$$

It depends on the effective mass flow, i.e. the injection rate $\dot{m}_{\text{inj}}$ and the corresponding mass fraction x_{inj}, the mass density of the solid ρ_{s}, the porosity of the particles' shell ϵ_{shell} and the overall surface of the particle bed

$$A_{\text{bed}}(t) = \pi \mu_2(n) \tag{3}$$

where μ_2 is the second moment of the particle size distribution n. The i-th moment is given as:

$$\mu_i(n) = \int_0^\infty L^i n(t,L)\, \mathrm{d}L. \tag{4}$$

As has been shown in experiments by Diez et al. (2018); Hoffmann et al. (2015); Rieck et al. (2015), the shell porosity ϵ_{shell} correlates linearly to the drying potential η for the layering granulation of sodium benzoate.

$$\epsilon_{\text{shell}} = -\Delta\epsilon_{\text{shell}} \eta + \epsilon_{\text{shell},0}\ . \tag{5}$$

Assuming an ideally mixed fluidization medium, the drying potential η is given by the moisture content of the fluidization medium at the inlet Y_{in}, inside the process chamber Y and its saturation moisture Y_{sat}.

$$\eta = \frac{(Y_{\text{sat}} - Y)}{(Y_{\text{sat}} - Y_{\text{in}})}\ . \tag{6}$$

During the continuous process operation particles are withdrawn from the granulation chamber.

$$\dot{n}_{\text{out}}(t,L) = Kn \tag{7}$$

The withdrawn particles are then classified into fines $\dot{n}_{\text{fines}}$, product $\dot{n}_{\text{product}}$, and oversized fraction $\dot{n}_{\text{over}}$ using a sieving box.

$$\dot{n}_{\text{over}} = T_1 \dot{n}_{\text{out}} \tag{8}$$

$$\dot{n}_{\text{product}} = (1-T_1) T_2 \dot{n}_{\text{out}} \tag{9}$$

$$\dot{n}_{\text{fines}} = (1-T_1)(1-T_2) \dot{n}_{\text{out}} \tag{10}$$

Here, T_1 and T_2 are the separation functions for the two sieves.

$$T_i = \frac{\int_0^L \exp\left(\frac{-(L-\mu_i)^2}{2\sigma_1^2)}\right)}{\int_0^\infty \exp\left(\frac{-(L-\mu_i)^2}{2\sigma_1^2)}\right)} \tag{11}$$

While the product fraction is removed from the process, oversized particles are milled and than fed back to the process together with the particles from the fines fraction. It is assumed that the mill generates a Gaussian size distribution with a mean diameter L_{mill} and variance σ^2_{mill}. The mass of the oversize fraction is hereby conserved.

$$\dot{n}_{mill} = 6 \frac{e^{-\frac{\left(L-L_{\text{mill}}\right)^2}{2\sigma_M^2}}}{\sqrt{2\pi}\pi\varrho\sigma_M} \int_0^\infty L^3 \dot{n}_{\text{over}} dL. \tag{12}$$

The particle flows $\dot{n}_{\text{in}}$ and $\dot{n}_{\text{out}}$ in eq. 1 are then given as follows:

$$\dot{n}_{\text{in}} = \dot{n}_{mill}, \tag{13}$$

$$\dot{n}_{\text{out}} = \dot{n}_{\text{product}} + \dot{n}_{\text{over}}. \tag{14}$$

In contrast to previous works, the mean diameter L_{mill} is assumed to consist of two terms: $L_{\text{mill},0}$ accounting for the mill operating conditions, e.g. the mill power, and ΔL_{mill} representing the influence of the particle properties on the breakage.

$$L_{\text{mill}} = L_{\text{mill},0} + \Delta L_{\text{mill}}\ . \tag{15}$$

As has been shown in Diez et al. (2018) the later, i.e. ΔL_{mill}, is strongly influenced by the apparent porosity ϵ_{p}.

$$\epsilon_{\text{p}} = 1 - \frac{m_{\text{p,dry}}/\rho_{\text{s}}}{(\pi/6)\, \mu_3(n(t,L))} \tag{16}$$

In the following, it will be assumed that this influence can be reflected by a linear correlation.

$$\Delta L_{\text{mill}}(\epsilon_{\text{p}}) = a_{\text{break}} + b_{\text{break}} \epsilon_{\text{p}} \tag{17}$$

In order to keep the bed mass constant over time a mass controller is applied using the drain K as a control handle.

This behavior can be reflected by an ideal mass controller, i.e. choosing the drain K such that the time-derivative of the bed mass vanishes.

$$K = -\frac{(1-\epsilon_{\text{shell}})\int_0^\infty L^3 G \frac{\partial n}{\partial L} dL}{(1-\epsilon_{\text{p}})\int_0^\infty L^3 \dot{n}_{\text{product}} dL}. \tag{18}$$

Assuming an ideally mixed system, the model equations for the fluid phase can be derived from the mass and enthalpy balances given in Neugebauer et al. (2018). The states are here the temperature, moisture content and mass of the particle and fluid phase, respectively. The moisture content of the particle and fluid phase, X and Y, are defined as the ratios of solvent to dry mass.

$$X = \frac{m_{p,solvent}}{m_{p,dry}} \tag{19}$$

$$Y = \frac{m_{f,solvent}}{m_{f,dry}} \tag{20}$$

The time behavior of the moisture contents is thus given by:

$$\dot{X} = \frac{\dot{m}_{p,solvent} - X\dot{m}_{p,dry}}{m_{p,dry}}, \tag{21}$$

$$Y = \frac{\dot{m}_{f,solvent} - Y\dot{m}_{f,dry}}{m_{f,dry}}, \tag{22}$$

where $\dot{m}_{p,solvent}$, $\dot{m}_{p,dry}$, $\dot{m}_{f,solvent}$, $\dot{m}_{f,dry}$ are the mass changes resulting from the mass balances for the solvent and the dry mass of the particle and fluid phase. The mass balances for the dry mass and solvent of the particle phase consist of the mass addition from the injected spray $x_{\text{inj}}\dot{m}_{\text{inj}}$ and $(1-x_{\text{inj}})\dot{m}_{\text{inj}}$, the external supply of particles $\dot{m}_{\text{p,dry,in}}$ and $X_{in}\dot{m}_{\text{p,dry,in}}$, e.g. external seeding particles with a moisture content X_{in}, and the product removal $\dot{m}_{\text{p,dry,out}}$ and $X\dot{m}_{\text{p,dry,out}}$. Furthermore, does the solvent mass balance of the particle phase contain a sink for the liquid evaporation $\dot{m}_{\text{evap}}$. The mass balances for the solvent and dry mass of the liquid phase contain the terms for the incoming and outgoing gas stream, $\dot{m}_{\text{f,dry,in}}$, $\dot{m}_{\text{f,dry,out}}$, $Y_{\text{in}}\dot{m}_{\text{f,dry,in}}$ and $Y\dot{m}_{\text{f,dry,out}}$, and the solvent supply from evaporation in the particle phase.

$$\dot{m}_{\text{p,dry}}(t) = x_{\text{inj}}\dot{m}_{\text{inj}} + \dot{m}_{\text{p,dry,in}} - \dot{m}_{\text{p,dry,out}} \tag{23}$$

$$\dot{m}_{\text{p,solvent}}(t) = (1-x_{\text{inj}})\,\dot{m}_{\text{inj}} + X_{\text{in}}\dot{m}_{\text{p,dry,in}} - X\dot{m}_{\text{p,dry,out}} - \dot{m}_{\text{evap}} \tag{24}$$

$$\dot{m}_{\text{f,dry}}(t) = \dot{m}_{\text{f,dry,in}} - \dot{m}_{\text{f,dry,out}} \tag{25}$$

$$\dot{m}_{\text{f,solvent}}(t) = Y_{\text{in}}\dot{m}_{\text{f,dry,in}} - Y\dot{m}_{\text{f,dry,out}} + \dot{m}_{\text{evap}} \tag{26}$$

Here, the mass flow rates $\dot{m}_{\text{p,dry,in}}$ and $\dot{m}_{\text{p,dry,out}}$ represent the coupling with the population balance model.

$$\dot{m}_{\text{p,dry},i} = (1-\epsilon_{\text{p},i})\,\rho_{\text{s}}\frac{\pi}{6}\int_0^\infty L^3\dot{n}_i dL \tag{27}$$

where $i = \{in, out\}$. The evaporation rate $\dot{m}_{\text{evap}}$ depends mainly on the overall surface of the particles, the drying velocity $\dot{\nu}$ and the difference between the liquid phase moisture content Y and its saturation level Y_{sat}. Here, the saturation moisture Y_{sat} reflects the maximum vapor amount which can be carried by the fluid. For the given granulation process it is a function of the inlet moisture content Y_{in} and temperature $\theta_{\text{f,in}}$, i.e. $Y_{\text{sat}} = Y_{\text{sat}}(Y_{\text{in}}, \theta_{\text{f,in}})$.

$$\dot{m}_{\text{evap}} = \dot{\nu}(\delta)\,\beta_{\text{fp}}(A_{\text{bed}}Y_{\text{sat}} - Y)\rho_{\text{f,dry}} \tag{28}$$

The coefficient β_{fp} describes the mass transport between fluid and particles as proposed in Gnielinski (2013). On the macroscopic scale the drying process can be divided into three stages (e.g. van Meel (1958)) shown in Fig. 2. Here, each stage depends on the particle moisture content X and its relation to the thermodynamic adsorption equilibrium X_{eq} and the critical particle moisture content X_{crit}:

(1) for a low moisture content X below the thermodynamic adsorption equilibrium X_{eq}, i.e. $X < X_{\text{eq}}$, no evaporation takes place, thus the normalized drying velocity $\dot{\nu}$ is zero,
(2) for moisture contents above the thermodynamic adsorption equilibrium, but below a certain critical moisture, i.e. $X_{\text{eq}} \leq X \leq X_{\text{crit}}$, the normalized drying velocity $\dot{\nu}$ increases with an increasing moisture content,
(3) if the moisture content X is greater than the critical particle moisture content X_{crit}, i.e. $X \geq X_{\text{crit}}$, the evaporation rate is limited by the state of the fluidization medium and the normalized drying velocity $\dot{\nu}$ is at its maximum, i.e. $\dot{\nu} = 1$.

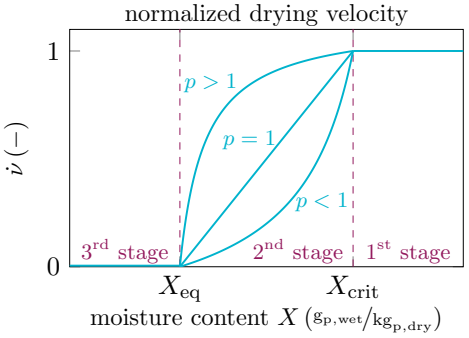

Fig. 2. Normalized drying velocity $\dot{\nu}$ over particle moisture content X

The described behavior is reflected using the normalized drying velocity (van Meel (1958)).

$$\dot{\nu}(\delta) = \begin{cases} 1 & \text{if } X \geq X_{\text{crit}} \\ \dfrac{p\delta(X)}{1+(p-1)\,\delta(X)} & \text{if } X_{\text{crit}} > X \geq X_{\text{eq}} \\ 0 & \text{if } X_{\text{eq}} > X \end{cases} \tag{29}$$

where $\delta(X) = \frac{(X-X_{\text{eq}})}{(X_{\text{crit}}-X_{\text{eq}})}$ represents the normalized moisture content. The differential equations for the fluid and particle temperature, $\dot{\theta}_{\text{f}}$ and $\dot{\theta}_{\text{p}}$, can be derived from the enthalpy balances for the fluid and particle phase (Neugebauer et al. (2018)). Due to the coupling between both phases and the number of input/output streams both equations are rather long and thus omit here.

The overall model, as depicted in Fig. 1, consists of the population balance equation for the particle size distribution and the equations describing the heat and mass

transfer between the particle bed and the gas phase. It should be mentioned, that most of the parameters and heuristic characteristics are subject to considerable uncertainty and vary with the operating conditions. This results in a corresponding large plant-model mismatch. Therefore, it is reasonable to incorporate appropriate uncertainties in the control design procedure.

3. CONTROLLER DESIGN

From an application point of view, it is of interest to control the Sauter diameter $d_{32,\mathrm{bed}}$, i.e. the ratio of the third and second moment of the particle size distribution, and the moisture content of the fluid phase η. The first gives is a measure for the average particle diameter, whereas the second describes the efficiency of the drying process.

As control handles the milling diameter $L_{\mathrm{mill},0}$ and the fluid inlet temperature $\theta_{\mathrm{f,in}}$ are used. Both can be easily actuated at the real plant. The resulting control problem is hence a 2x2 MIMO system, where the coupling is due to the bidirectional dependencies between the particle and fluid phase. The nonlinear system model has been discretized using a finite volume scheme and linearized at a operating point. The resulting 2×2 transfer function $G(s)$ depicted in Fig. 3 is of order 208 and has thus been further reduced using balanced model truncation (Fig. 4).

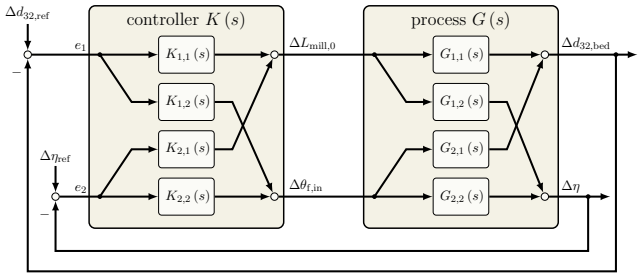

Fig. 3. MIMO control scheme

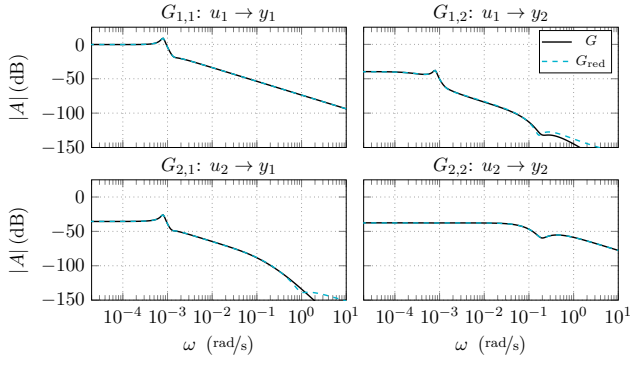

Fig. 4. Bode plots of the full-order transfer function $G(s)$ and the reduced system $G_{\mathrm{red}}(s)$.

The resulting 8-th order transfer function has been used as the nominal model for control design. In order to cope for the above described uncertainties a set of transfer functions for different operating points and parameters has been derived. The maximum and minimum singular value of the resulting transfer functions and the chosen nominal system are depicted in Fig. 5. Calculating the relative deviations to nominal systems, results in the according multiplicative errors, which have been overestimated by a low order transfer function Δ_M representing an unstructured multiplicative output model uncertainty (Fig. 5).

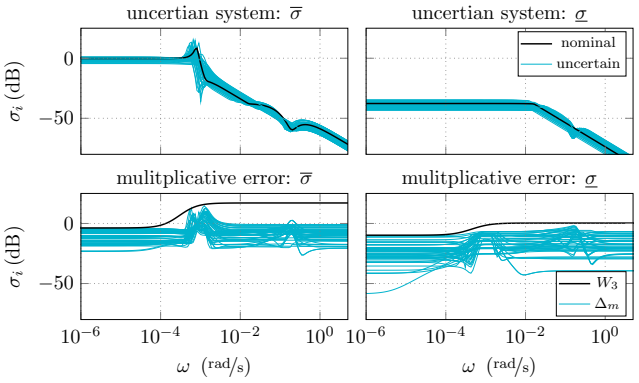

Fig. 5. Singular values of the open-loop frequency response of the uncertain system (upper row) and the corresponding multiplicative model uncertainty (lower row).

In order to design a controller, which robustly stabilizes the given uncertain process, the H_∞-mixed sensitivity approach will be used. Here, the multiplicative output uncertainty Δ_M is taken into account using the weighting of the complementary sensitivity $W_3(s)$. Nominal performance requirements, e.g. steady-state error, can be introduced using the weighting of the sensitivity $W_1(s)$. Restrictions on the control can be reflected by weighting KS using $W_2(s)$. The respective design requirements are fulfilled if a stabilizing controller K can be calculated minimizing the following H_∞-problem such that its H_∞-norm is smaller than 1, i.e. $\gamma < 1$.

$$\min_{K \text{ stabilize}} \left\| \begin{matrix} S(s) W_1(s) \\ K(s) S(s) W_2(s) \\ T(s) W_3(s) \end{matrix} \right\|_\infty \leq \gamma \tag{30}$$

The generalized structure of the given H_∞-based mixed-sensitivity design problem is shown in Fig. 6.

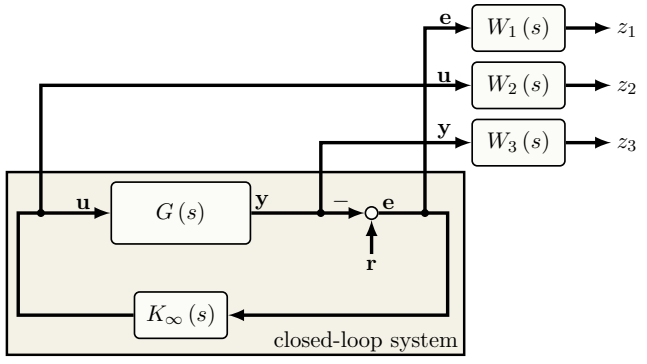

Fig. 6. Structure of the H_∞-mixed-sensitivity design problem.

For convenience two different types of weighting functions W_{I} and W_{II} have been used.

	W_1	$W_{2,1}$	$W_{2,2}$	$W_{3,1}$	$W_{3,2}$
Typ	W_I	W_II	W_II	W_II	W_II
A	5.0×10^{-3}	1.0×10^{-4}	$2.0 \times 10^{+3}$	4.0×10^{-1}	3.25×10^{-1}
ω_b	7.5×10^{-5}	—	—	—	—
M	$1.5 \times 10^{+0}$	—	—	—	—
T	—	$1.0 \times 10^{+0}$	$1.0 \times 10^{+0}$	$3.5 \times 10^{+3}$	$1.25 \times 10^{+3}$
T_D	—	$1.0 \times 10^{+3}$	$2.0 \times 10^{+3}$	$7.5 \times 10^{+3}$	$4.0 \times 10^{+3}$
n	—	1	1	4	1

Table 1. Weighting parameters

$$W_\mathrm{I}(s) = \frac{(T_\mathrm{p} s + 1)}{(M T_\mathrm{p} s + A)} \quad \text{with} \quad T_\mathrm{p} = {}^1/_{\omega_\mathrm{b} M} \tag{31}$$

$$W_\mathrm{II}(s) = \frac{A\,(T_\mathrm{d} s + 1)^n}{(T s + 1)^n} \tag{32}$$

The chosen parameters are given in Table 3. Here, diagonal weightings have been chosen, where the second index defines the element on the diagonal, e.g. $W_{2,1}$ is the upper left element of the weighting matrix W_2. For W_1 equal weightings have been chosen for both channels.

Solving the mixed-sensitivity H_∞-problem (eq. 30) for the chosen nominal plant and the weightings, yields a H_∞-controller. The resulting closed-loop singular values in comparison to the according weighting functions are depicted in Fig. 7. As can be seen, the design requirements are fulfilled.

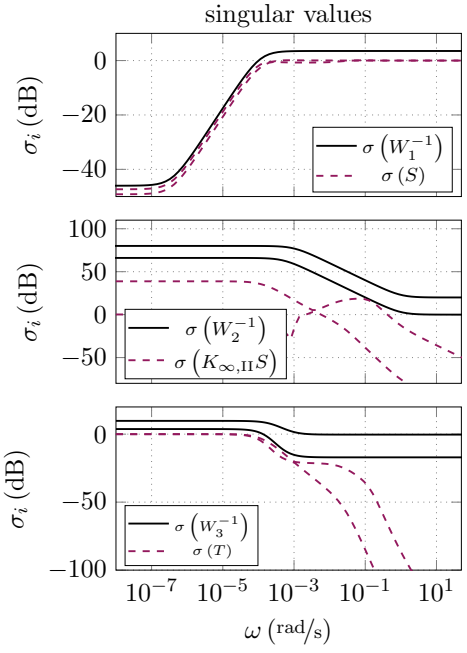

Fig. 7. Singular values of the closed-loop transfer functions $S(s)$, $T(s)$, and $K(s)S(s)$ compared to the weighting functions $W_i(s)$.

4. SIMULATION RESULTS

In order to test the designed robust controller simulations with the full nonlinear model are provided. Here, two scenarios of practical relevance have been chosen. In the first scenario at time $t_\mathrm{sp} = 2$ h the reference value of the particle porosity $\epsilon_\mathrm{p,ref}$ is increased from 0.39 to 0.425. After that at time $t_\mathrm{dist} = 15$ h the moisture content Y_in changes due to an external disturbance from 6 ${}^{\mathrm{g_{f,wet}}}/_{\mathrm{kg_{f,dry}}}$ to 15 ${}^{\mathrm{g_{f,wet}}}/_{\mathrm{kg_{f,dry}}}$. The results for the controlled outputs and the control action are shown in Fig. 9. The according particle size distribution is depicted in Fig. 8. As can be seen, the process remains stable and the output values follow their set-points with smaller oscillations in the Sauter diameter. The control effort is reasonable and the external disturbance is well-suppressed.

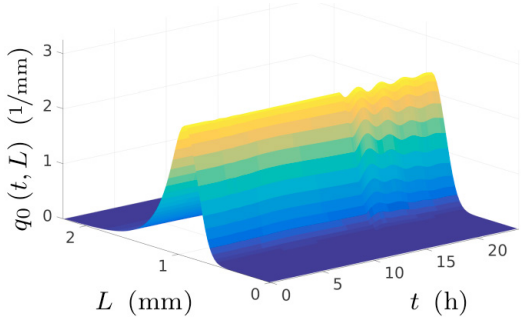

Fig. 8. Normalized particle size distributions $q_0(t, L)$ (scenario 1)

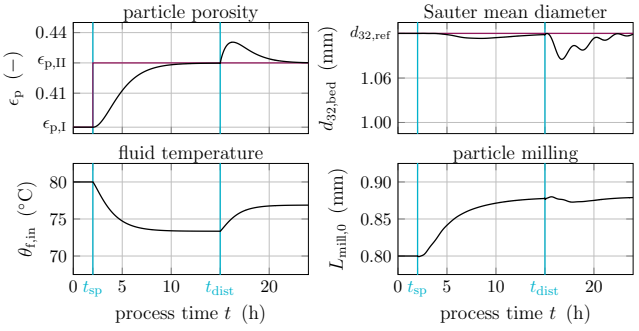

Fig. 9. Controlled outputs and control action during (scenario 1)

In the second scenario, the reference value of particle porosity $\epsilon_\mathrm{p,ref}$ is increased from 0.39 to 0.425 at time $t_\mathrm{sp} = 2$ h. However, at time $t_\mathrm{dist} = 15$ h, the injection rate $\dot{m}_\mathrm{inj}$ is decreased from 40.0 kg/h to 34.0 kg/h, which has a direct influence on the particle growth rate. The resulting particle size distribution is shown in Fig. 10. Again the controlled outputs and the control action stay within reasonable limits (Fig. 11).

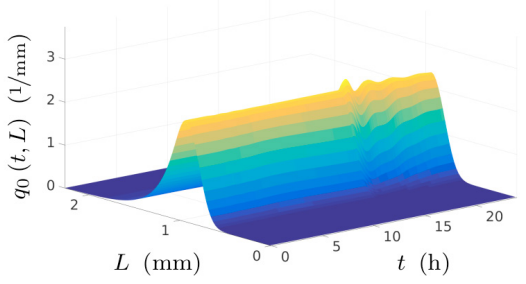

Fig. 10. Normalized particle size distributions $q_0(t, L)$ (scenario 2)

5. CONCLUSION

A robust controller has been designed for a fluidized bed layering granulation with external sieve-mill-cycle. From

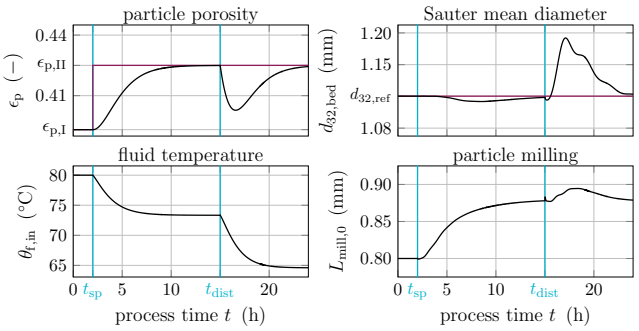

Fig. 11. Controlled outputs and control action during (scenario 2)

a practical point of view, it is important to guarantee certain product properties as for example particle size or porosity. Due to the strong coupling between the particle and fluid phase, external disturbances and high process uncertainties, this is a challenging task. As has been shown in this contribution the H_∞-mixed-sensitivity control approach allows for a reasonable solution of this problem. The set-point and disturbance scenarios are of practical relevance and represent typical challenges in production.

ACKNOWLEDGEMENTS

The financial support of DFG (Deutsche Forschungsgemeinschaft) within the priority program SPP1679 (project number: Kl 417/3-3) and by the European Regional Development Fund (ERDF) within the Center of Dynamic Systems is gratefully acknowledged.

REFERENCES

Cotabarren, I.M., Bertín, D.E., Bucalá, V., and Piña, J. (2015). Feedback control strategies for a continuous industrial fluidized-bed granulation process. *Powder Technology*, 283, 415 – 432.

Diez, E., Meyer, K., Bück, A., Tsotsas, E., and Heinrich, S. (2018). Influence of process conditions on the product properties in a continuous fluidized bed spray granulation process. *Chemical Engineering Research and Design*, 139, 104 – 115.

Dreyschultze, C., Neugebauer, C., Palis, S., Bück, A., Tsotsas, E., Heinrich, S., and Kienle, A. (2015). Influence of zone formation on stability of continuous fluidized bed layering granulation with external product classification. *Particuology*, 23, 1–7.

Gnielinski, V. (2013). G9 - Wärmeübertragung Partikel - Fluid in durchströmten Haufwerken. In *VDI Wärmeatlas*. VDI Verlag.

Hoffmann, T., Rieck, C., Schmidt, M., Bück, A., Peglow, M., and Tsotsas, E. (2015). Prediction of shell porosities in continuous fluidized bed spray layering. *Drying Technology*, 33(13), 1662–1670.

Mörl, L., Heinrich, S., and Peglow, M. (2007). Handbook of powder technology, fluidized bed spray granulation. 21 – 188.

Neugebauer, C., Diez, E., Bück, A., Palis, S., Heinrich, S., and Kienle, A. (2019). On the dynamics and control of continuous fluidized bed layering granulation with screen-mill-cycle. *Powder Technology*, 354, 765 – 778.

Neugebauer, C., Palis, S., Bück, A., Tsotsas, E., Heinrich, S., and Kienle, A. (2017). A dynamic two-zone model of continuous fluidized bed layering granulation with internal product classification. *Particuology*, 31, 8 – 14.

Neugebauer, C., Bück, A., Palis, S., Mielke, L., Tsotsas, E., and Kienle, A. (2018). Influence of thermal conditions on particle properties in fluidized bed layering granulation. *Processes*, 6(12).

Palis, S. (2018). Non-identifier-based adaptive control of continuous fluidized bed spray granulation. *Journal of Process Control*, 71, 46 – 51.

Palis, S. and Kienle, A. (2012). Stabilization of continuous fluidized bed spray granulation with external product classification. *Chemical Engineering Science*, 70, 200 – 209.

Palis, S. and Kienle, A. (2014). Discrepancy based control of particulate processes. *Journal of Process Control*, 24, 33 – 46.

Palis, S. and Kienle, A. (2013). H_∞ loop shaping control for continuous fluidized bed spray granulation with internal product classification. *Industrial & Engineering Chemistry Research*, 52(1), 408–420.

Rieck, C., Hoffmann, T., Bück, A., Peglow, M., and Tsotsas, E. (2015). Influence of drying conditions on layer porosity in fluidized bed spray granulation. *Powder Technology*, 272, 120 – 131.

Schmidt, M., Bück, A., and Tsotsas, E. (2017). Experimental investigation of the influence of drying conditions on process stability of continuous spray fluidized bed layering granulation with external product separation. *Powder Technology*, 320(Supplement C), 474 – 482.

van Meel, D. (1958). Adiabatic convection batch drying with recirculation of air. *Chemical Engineering Science*, 9(1), 36 – 44.